

Second-harmonic imaging microscopy of living cells

Paul J. Campagnola

Heather A. Clark

William A. Mohler

Center for Biomedical Imaging Technology
University of Connecticut Health Center
263 Farmington Avenue
Farmington, Connecticut 06030

Aaron Lewis

Division of Applied Optics
Hebrew University
Jerusalem
Israel

Leslie M. Loew*

Center for Biomedical Imaging Technology
University of Connecticut Health Center
263 Farmington Avenue
Farmington, Connecticut 06030

Abstract. Second harmonic generation (SHG) has been developed in our laboratories as a high-resolution nonlinear optical imaging microscopy for cellular membranes and intact tissues. SHG shares many of the advantageous features for microscopy of another more established nonlinear optical technique: two-photon excited fluorescence (TPEF). Both are capable of optical sectioning to produce three-dimensional images of thick specimens and both result in less photo-damage to living tissue than confocal microscopy. SHG is complementary to TPEF in that it uses a different contrast mechanism and is most easily detected in the transmitted light optical path. It can be used to image membrane probes with high membrane specificity and displays extraordinary sensitivity in reporting membrane potential; it also has the ability to image highly ordered structural proteins without any exogenous labels. © 2001 Society of Photo-Optical Instrumentation Engineers. [DOI: 10.1117/1.1383294]

Keywords: two-photon excitation; membrane potential; gold nanoparticles; fluorescence lifetime; collagen.

Paper FM-08 received Apr. 2, 2001; accepted for publication Apr. 20, 2001

1 Introduction

In this article we present a summary of our recent work as well as some new results using second harmonic generation (SHG) as a high-resolution nonlinear optical imaging tool (SHIM) for cellular membranes and intact tissues. SHG is a second order nonlinear optical process that can only arise from media lacking a center of symmetry, e.g., an anisotropic crystal or at an interface such as a membrane. Since SHG is a nonlinear optical phenomenon, it shares many of the features of two-photon excited fluorescence (TPEF) microscopy. The popularity of TPEF has greatly expanded since the first implementation for biological microscopy in 1990¹ and has found useful applications in neuroscience, cell biology, and biophysics. Due to greatly reduced out-of-plane photobleaching and phototoxicity, this methodology has gained considerable popularity as an ideal method for live cell imaging. In addition, the use of near infrared excitation results in the ability to penetrate deeply into turbid and thick tissue because of reduced light scattering and reduced absorption by intrinsic chromophores. A comprehensive coverage of recent work is beyond the scope of this article.^{2–9} SHG is complementary to TPEF. It can be used to image membrane probes with high membrane specificity and high sensitivity in reporting membrane potential; it also has the ability to image highly ordered structural proteins without any exogenous labels.

In general, the nonlinear polarization for a material can be expressed as

$$P = \chi^{(1)}E^1 + \chi^{(2)}E^2 + \chi^{(3)}E^3 + \dots, \quad (1)$$

where P is the induced polarization, $\chi^{(n)}$ is the n th order nonlinear susceptibility, and E is the electric field vector of the incident light. The first term describes normal absorption and reflection of light, the second, SHG, sum, and difference

frequency generation, and the third, both two and three photon absorption, as well as third harmonic generation. SHG was first demonstrated in crystalline quartz in 1962 by Kleinman¹⁰ and since that time has been commonly used to frequency double pulsed lasers to obtain shorter wavelengths. Shortly thereafter, SHG from interfaces was discovered by Bloembergen 1968¹¹ and since has become a standard spectroscopic tool for characterizing surfaces and probing dynamics at interfaces (for reviews, see Shen¹² and Eienthal¹³). In 1974, Hellwarth integrated SHG into an optical microscope to visualize the microscopic crystal structure in polycrystalline ZnSe.¹⁴ This concept was demonstrated in both the 1970s and again in the 1990s with more modern imaging equipment and laser sources and as well as extended to three dimensions by Sheppard.^{15,16} Here we present results of our SHIM efforts on live tissue culture cells, animal tissue, and examining the SHG enhancements arising from metallic nanoparticles interacting with dyes at cellular membranes. A major advance of our efforts has been the implementation of SHG into a laser scanning optical microscope where images can be obtained with comparable pixel density and frame rates as confocal or two-photon fluorescence microscopy.

To the best of our knowledge, the first biological SHG imaging experiments were by Freund et al. in 1986.¹⁷ They utilized SHG to study the orientation of collagen fibers in rat tail tendon at approximately 50 μm resolution. In the first use of SHG to examine biological membranes, Lewis and Shen determined the change in dipole moment of bacteriorhodopsin.¹⁸ Our laboratories used a hemispherical bilayer apparatus to measure the electric field sensitivity of SHG arising from a voltage sensitive dye.¹⁹ Subsequently, SHG measurements were used to monitor membrane potential responses following stimulation of photoreceptor cells by visible light.²⁰ More recently, we modified a laser scanning two-photon microscope to obtain SHG images with similar pixel

*Address all correspondence to L. M. Loew. Tel: 860-679-3568; Fax: 860-679-1039; E-mail: les@volt.uconn.edu

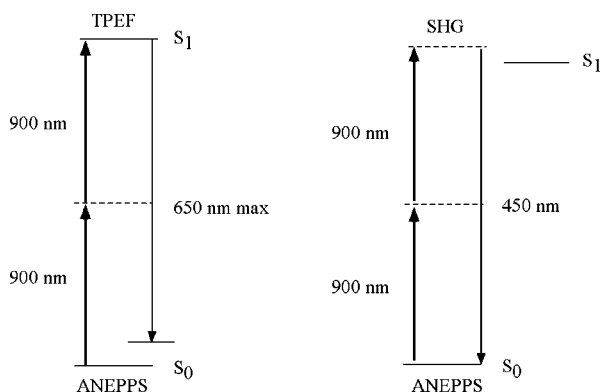


Fig. 1 Jablonski diagram showing the photophysical processes for the ANEPPS chromophore using two-photon excited fluorescence (left) and second harmonic generation (right). The approximate absorption and emission maxima are shown for TPEF.

density as that of a standard confocal microscopy with similar acquisition rates.²¹ For increased contrast, the cells are stained with potential sensitive styryl dyes [naphthylstyryl chromophore] that possess large second order optical nonlinearities. The achievable resolution and contrast were demonstrated with N1E-115 neuroblastoma cells, NIH 3T3 fibroblasts, and L1210 lymphocytes. Since a membrane is a bilayer and thus not a simple interface, we used several forms of these dyes consisting of the same styryl chromophore but having different alkyl chain lengths and chirality to study mechanisms and efficiency of contrast generation. SHIM of these dyes is highly sensitive to membrane potential, significantly greater than that of fluorescence methods. We have also investigated the interaction of the ANEP dyes with gold and silver nanoparticles; novel dye-nanoparticle conjugates lead to greatly enhanced SHG signals relative to the dye alone. In a final section we will present preliminary data on SHG imaging of collagen in zebrafish scales at approximately 1 μm resolution at frame rates on the 1 s time scales. We first begin with a description of the physical background of SHG and compare the photophysics to the more familiar process of two-photon excited fluorescence.

2 Physical Background

The processes of two-photon excited fluorescence (left) and second harmonic generation (right) are shown in the Jablonski diagram in Figure 1. Consider the case of the ANEPPS naphthylstyryl chromophore bound to a cell membrane. This dye has a one photon absorption and emission maximum in lipid of about 450 and 650 nm, respectively. Alternatively, excitation can occur via two-photon absorption at 900 nm, where the chromophore is simultaneously excited from the ground state, S_0 , through a virtual state to the first excited state S_1 . The resulting emission spectrum will be the same for both excitation modes since relaxation is independent of the excitation pathway; thus two-photon excitation will also produce emission at 650 nm. SHG, by contrast, does not arise from an absorptive process. Instead, an intense laser field induces a nonlinear, second order, polarization in the assembly of molecules, resulting in the production of a coherent wave at exactly twice the incident frequency (or half the wavelength).

The spectral and temporal profiles of two-photon excited fluorescence and SHG are also very different. In the former, the width of the emission spectrum is determined by the relative geometries of the ground and excited state and the emission lifetime is related to the oscillator strength and is typically on the order of a few nanoseconds. It should be noted that these properties are independent of the characteristics of the excitation laser characteristics. In SHG, by contrast, both the spectral and temporal characteristics are derived from the laser source: the bandwidth scales as $1/\sqrt{2}$ of the bandwidth of excitation laser, and, due to the coherence of the process, the SHG pulse is temporally synchronous with the excitation pulse.

A major constraint of SHG is the requirement of a noncentrosymmetric environment. This is readily understood by inspection of Eq. (2) in terms of the electric dipole expansion

$$P = \chi^{(2)} EE, \quad (2)$$

where the polarization and electric field are vector quantities. Since the SHG wave is a vector quantity, the induced polarization in a centrosymmetric sample from all directions would be equal and opposite and vector sum to zero. However, because a membrane is a liquid-liquid interface, both intracellular organelle and plasma membranes are suitable samples to be probed with this methodology. This is because the membrane structure forces a noncentrosymmetric environment, provided only one leaflet is stained. Conversely, this technique is not amenable to probing cytosolic dynamics. SHG can also result from an electric quadrupole interaction from samples with a large change in optical dielectric constant at the interface, e.g., at a metal surface. This interaction obviates the requirement for a nonsymmetric environment, however, it is expected to be very small for biological samples.

Next we examine the parameters that define the SHG signal. Equation (3) is a simplified expression for the relationship, which in its full form is a complex tensor equation.

$$I(2\omega) \propto \left[\chi^{(2)} \frac{P}{\tau}(\omega) \right]^2 \tau, \quad (3)$$

where $\chi^{(2)}$ is the second order nonlinear susceptibility, P is the pulse energy, and τ is the laser pulse width. As in TPEF, the signal is quadratic with peak power, but since SHG is an instantaneous process, a signal will only be generated during the duration of the laser pulse. Thus, although derived from different physics, SHG has the same inverse dependence on the laser pulse width as two-photon excitation. $\chi^{(2)}$ is the macroscopic version of β , the first hyperpolarizability (a molecular property) and is related by

$$\chi^{(2)} = N_s \langle \beta \rangle, \quad (4)$$

where N_s is the density of molecules and the brackets denote an orientational average. This further underscores the need for a noncentrosymmetric region, since $\langle \beta \rangle$ would vanish for an isotropic distribution of dipole moments.

Examination of Eqs. (3) and (4) also reveals a major difference in the expected contrast for the TPEF and SHG signal levels: SHG depends on the square of the surface density whereas fluorescence intensity is linear with the density of fluorophores. This can lead to significant differences in these

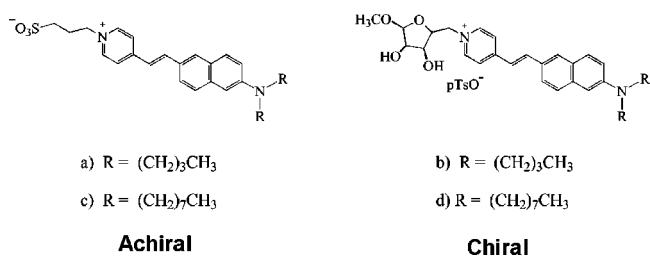


Fig. 2 The chemical structures of the voltage sensitive dyes used in this work. The R alkyl group anchors the dye in the membrane and the addition of the chiral sugar group (right structure) enhances the SHG by approximately twofold.

two mechanisms even when the signal only arises from the same dye in the membrane. For example, at high dye concentrations the fluorescence signal will become quenched due to dye aggregation and subsequent nonradiative decay, while the SHG would actually be larger due to the square dependency on the surface density.

An overriding concern in all biological imaging is optimizing sensitivity and avoiding photodamage. This is especially true when dealing with nonlinear forms of excitation since new photodamage pathways become possible even while out-of-focus damage is reduced. These can include, for example, three photon excitation of nucleic acids and proteins. Thus the design of efficient dyes is of paramount importance, so that minimal laser power can be used to obtain useful images. The investigation of chemical properties leading to large second (SHG) and third order (TPEF) nonlinear optical properties is currently an active area of research.^{22–30} While specifics vary between classes of molecules, some generalizations are becoming apparent. Typically, dyes that have extended conjugated π networks have excellent second and third order characteristics. Further, dyes with push–pull character, i.e., possessing intramolecular electron donor–acceptor (DA) pairs also give rise to nonlinear optics (NLO) enhancements. Aromatic heteroatom (nitrogen or sulfur) substitution further increases the DA interaction. For example, rhodamine B differs in structure from fluorescein primarily only by a nitrogen substitution but has a 20-fold larger two-photon absorption cross section. Lastly, within the two-level system model, the second order hyperpolarizability, β , i.e., the molecular version of $\chi^{(2)}$, and thus SHG efficiency is given by

$$\beta = \frac{3e^2}{2\hbar^3} \frac{\omega_{ge} f_{ge} \Delta\mu_{ge}}{[\omega_{ge}^2 - \omega^2][\omega_{ge}^2 - 4\omega^2]}, \quad (5)$$

where e is electron charge, ω_{ge} , f_{ge} , and $\Delta\mu_{ge}$ are the energy difference, oscillator strength, and change in dipole moment between the ground and excited states, respectively.³¹ A simple styryl chromophore, ASP, has a change in dipole moment of approximately 16 D between the ground and excited states.³² The ANEP chromophore is expected to have a $\Delta\mu_{ge}$ at least as large and possess both large second and third order responses. The ANEP chromophore (shown in Figure 2) we use in our measurements is a strongly donating dialkylaminonaphthyl group and an electron accepting pyridinium nucleus, thus certainly satisfying all the above criteria. These properties should make styryl dyes ideal stains for both TPEF and

SHIM. Both the two-photon absorption cross section and first hyperpolarizability of this chromophore are larger than Rhodamine B, which is often a benchmark for performance. Other styryl chromophores have also been reported to have large second order nonlinear optical susceptibilities.^{23,24}

For our work we tested several naphthylstyryl (ANEP) dyes, including specially designed SHG dyes with covalently linked chiral sidechains (exemplified on the right side of Figure 2). While β would be expected to be the same for all dyes with the same ANEP chromophore, one might predict that the orientationally averaged ensemble, $\langle\beta\rangle_{OR}$, might be larger for chiral dyes. Indeed, these chiral dyes provided significantly larger (approximately twofold) SHG signal levels.^{19,21} The class of styryl chromophore used here was developed as a voltage sensor to measure membrane potential. The fact that the same molecular property, namely a large charge shift upon excitation [Eq. (5)], is responsible for both the sensitivity of the dye spectra to electric fields and the enhancement of SHG led us to investigate the possibility that the SHG signal might itself be sensitive to membrane potential.

While SHG is not an absorptive process, the magnitude of the SHG wave can be resonance enhanced when the energy of the second harmonic signal overlaps with an electronic absorption band.³³ Inspection of Eq. (5) shows that β becomes large when the laser fundamental frequency approaches the electronic transition. Then the total second order response is a sum of the nonresonant and resonant contributions:

$$\chi_{total}^{(2)} = \chi_{nonres}^{(2)} + \chi_{res}^{(2)}. \quad (6)$$

Depending upon the specific properties of the chromophore and the excitation wavelength, the resonant contribution can dominate, resulting in enhancement of an order of magnitude or more. Most of the work here is performed in this regime in order to generate sufficient contrast.

To further enhance the available contrast in SHIM, we have begun to examine the effects of SHG signals when these dyes interact with metallic nanoparticles. It has been known for some time that second harmonic generation (SHG) can be greatly enhanced ($\sim 10^4$) for dye molecules adsorbed on a roughened metal surface.³⁴ Similarly, very large enhancements ($\sim 10^6$) have been observed in surface enhanced Raman scattering (SERS) of organic dyes on several metallic surfaces.³⁵ More recently, these enhancements have been observed at the single particle level as well.³⁶ We have now developed a new type of dye-nanoparticle where the ANEP chromophore is linked to a polymer coated gold colloid via a succinimidylyl ester. We will present data on SHG enhancements arising from these particles and describe the photophysics.

3 Experimental Design Considerations

Our SHG imaging system is built on a modified laser scanning microscope and uses a titanium sapphire mode-locked laser as the excitation source.²¹ Unlike fluorescence, SHG is a coherent process and the signal copropagates in the forward direction and is detected in a transmitted light configuration. The numerical apertures used ranged between 0.8 and 1.3 NA.

A unique feature of this microscope is the ability to simultaneously collect the SHG and the TPEF signals, where the latter is acquired in the usual epi-illumination geometry. This

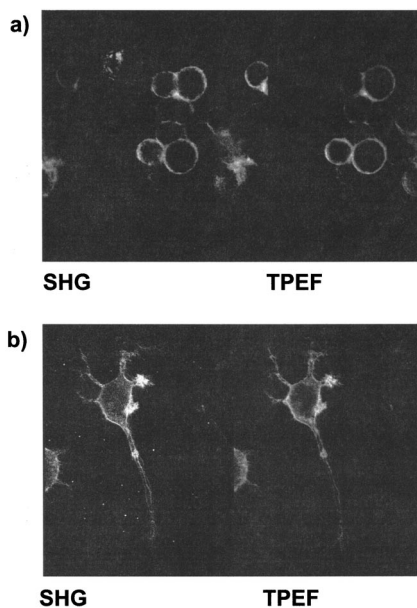


Fig. 3 Representative SHG and TPEF images of N1E-115 neuroblastoma cells, where the top and bottom show undifferentiated and differentiated cells, respectively. Data acquisition times were approximately 1 s.

allows for a direct comparison of these two contrast modalities, and further, allows the use of the TPEF as a normalization factor between samples to correct for different preparations. We make use of this scheme throughout the results reviewed here.

We have also utilized SHG to perform ensemble-averaged measurements to assess the performance of different dyes as well as the sensitivity to membrane potential. This has been achieved by using suspensions of L1210 lymphocytes and performing ratiometric measurements of the SHG and TPEF signals dispersed through a monochromator.

4 Results and Discussion

Our first imaging targets were neuroblastoma N1E-115 cells. These cells are good model neurons in terms of their differentiation and excitability. In addition, the fluorescence of these cells stained with the ANEP chromophore has been well-characterized by this laboratory, and are thus a good system in which to compare the TPEF and SHG images in terms of contrast and resolution. Figures 3(a) and 3(b) show the respective SHIM and TPEF of undifferentiated and differentiated cells, respectively, stained with the dye in Figure 2(d). Typical data are the result of three Kalman averages and required 3 s total acquisition time to reduce high frequency background light levels. These images were acquired using a 40×0.8 NA lens for the excitation. The field size is $330 \times 220 \mu\text{m}$ and composed of 768×512 pixels. A first inspection of these images indicates that the SHG and TPEF images carry the same information, i.e., in both cases the signal appears largely at the plasma membrane with some internal staining. The cell in Figure 3(b) shows the common features of differentiated neuronal cells: the soma, neurites, growth cones, and filopodia are all apparent. On a qualitative level, the resolution and contrast of TPE fluorescence and SHG are

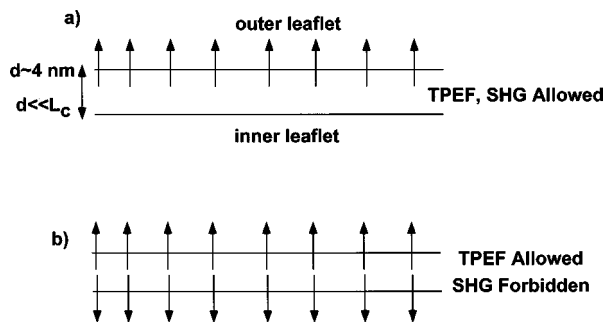


Fig. 4 Cartoon depicting single leaflet (a) and double leaflet staining (b). The alignment of dipole moments of the dye in the membrane is well-ordered.

similar. To a first approximation, this result is expected, since in both cases the contrast arises from the same chromophore staining the membrane, and the optical resolution limit for both processes should be governed by the excitation wavelength. A more careful inspection of many data sets has revealed slight differences between the two contrast mechanisms at isolated regions of these cells. It is unclear at this point if such differences are physiological, e.g., arising from differences in membrane potential or other unknown causes. A second possibility is if there is uneven staining of the membrane, differences could occur due to the linear (TPEF) versus quadratic (SHG) dependencies on surface density of dye molecules.

Having established that we can obtain high-resolution SHIM images with acquisition rates on the time scale of seconds, it is of interest to understand, at the molecular level, the mechanism of contrast generation. Although SHG has been used for almost 30 years to study processes at a variety of interfaces, a biological membrane is more complex because the two leaflets form two interfaces. Thus we must differentiate between contrast arising from single and double leaflet staining; a cartoon of these cases is shown in Figure 4, where the dye dipoles are well-aligned in the leaflets. Polarization anisotropy data from both SHG and TPEF (unpublished) bears out this condition as does earlier studies in monolayers.²² For staining of only the outer leaflet, both SHG and TPEF are expected. However, for equal staining of both leaflets, the situation is expected to be quite different. The TPEF is still allowed; however, within the electric dipole approximation the SHG signal should vanish. This is because the membrane thickness is approximately 4 nm, which is much shorter than the coherence length, L_c . This limit is on the order of the excitation wavelength and is approximated by

$$\Delta k \cdot L_c \sim \pi, \tag{7}$$

where Δk is the difference in wave vectors between the fundamental and second harmonic wavelengths. More specifically, if both the inner and outer leaflets of a membrane are equally stained, the second harmonic waves from each leaflet will be equal and opposite in direction and sum to zero. We can experimentally realize this scenario and examine the outcome by staining and imaging NIH 3T3 fibroblasts. These flat cells internalize membrane staining dyes relatively rapidly, resulting in equal double leaflet staining. Further, the cells

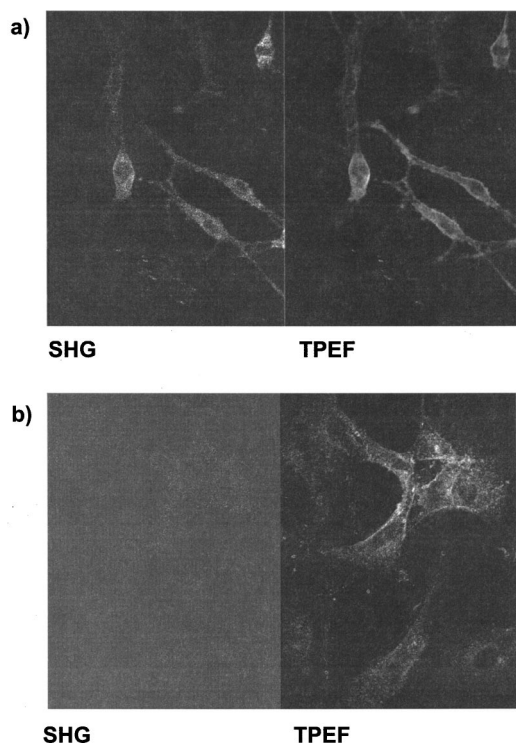


Fig. 5 SHG and TPEF images of NIH 3T3 fibroblasts. Cells in the top panel and bottom panel were stained with the dyes in Figures 2(b) and 2(a), respectively. These images were obtained using a 1.3 NA objective.

were stained with the shorter alkyl chain dyes Di-4-ANEPPS [Figure 2(a)] and JPW-1259 [Figure 2(b)] that are known to internalize faster than the Di-8 analogs.³⁷ The SHIM and TPEF data for the achiral and JPW-1259 chiral dye are shown in Figures 5(b) and 5(a), respectively. As with the two prior cell lines, the images are essentially identical but now widespread internal membrane staining is also observed. As expected, for the achiral dye, a strong TPEF image is observed (TPEF is not phase sensitive) and the SHG essentially is absent. Mertz and coworkers³⁸ obtained a similar result in imaging two bordering cell-size lipid vesicles stained with a styryl chromophore. However, the situation for the chiral dye is quite different, in that the SHG still persists, suggesting a much stronger dependence on the presence of a chiral center than would be predicted from the relative $\chi^{(2)}$ values (only twofold).²¹ We conclude from these sets of experiments, that in a membrane, the presence of a chiral center relaxes the requirement of the electric dipole “selection rule” that the assembly of molecules is noncentrosymmetric.

4.1 Potential Measurements

We alluded earlier to the large sensitivity that SHG has in probing membrane potential through the use of voltage sensitive dyes. As previously discussed, the large change in dipole moment that gives rise to Stark shifted electronic states also leads to large second harmonic signals. This was demonstrated first on a hemispherical bilayer apparatus, and encouraged by this success, SHG was then used to probe potential from cellular membranes stained with these dyes.^{20,21} In a simple experiment, the transmembrane potential was changed

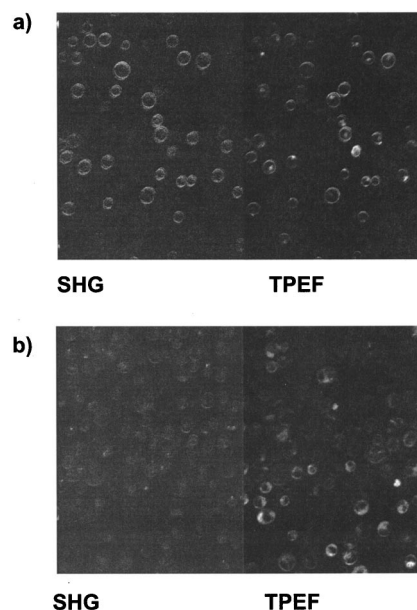


Fig. 6 SHG imaging to determine changes in membrane potential in L1210 lymphocytes labeled with dye in Figure 2(d). The cells in the top panel were in a normal buffer and those in the bottom were in a high potassium buffer (135 mM K⁺).

by varying the potassium concentration. Using the SHG/TPEF ratiometric idea described earlier, quantitative measurements were made of SHG efficiency in L1210 cell suspensions stained with JPW2080 [Figure 2(d)] upon membrane depolarization. Measurements were performed in samples of both normal ($[K^+] = 5$ mM) and high potassium buffer (135 mM). The analogous experiment was performed at the single cell level by SHIM; representative data are shown in Figure 6, where the top and bottom SHG and TPEF pairs correspond to normal buffer and high potassium, respectively. The cell suspensions showed

$$\left(\frac{\text{SHG}}{\text{TPEF}} \right)_{\text{low } K^+} ; \left(\frac{\text{SHG}}{\text{TPEF}} \right)_{\text{high } K^+}$$

normalized ratios of 2.1 ± 0.4 and imaging data (integrating on a cell by cell basis) on 30 trials showed 2.3 ± 0.6 . Confocal fluorescence imaging of TMRE, a Nernstian indicator,^{39,40} showed that this concentration of K⁺ led to a depolarization of approximately 25 mV in these cells. By contrast, fluorescence based ratiometric determinations with JPW2080 would have yielded a change of only a few percent for this change in potential. These results demonstrate that membrane potential measurements using SHG can be implemented on a laser-scanning microscope on physiologically relevant time scales. Further, this is seen as a unique aspect of SHIM relative to two-photon excited fluorescence.

While it is not within the scope of this article to fully elucidate the underlying theoretical basis, we can provide a physical picture of this sensitivity. It is well known from both the electrochemistry⁴¹ and physics literature⁴² that SHG intensities can be modulated by strong, static electric fields. The cell membrane can be considered an interface between two

immiscible electrolyte solutions and in such a system the total second order response can be represented by the following expression:

$$\chi_{\text{total}}^{(2)} = \chi_{\text{surface}}^{(2)} + \chi^{(3)} E_{\text{dc}}, \quad (8)$$

where $\chi_{\text{surface}}^{(2)}$ arises from the structural asymmetry of the interface, i.e., the membrane itself, E_{dc} is a static electric field, and $\chi^{(3)}$ is the third order susceptibility. Third order coefficients are generally on the order of four to five orders of magnitude smaller than $\chi^{(2)}$ and the second term in Eq. (8) is often negligible. However, given typical intramembrane electric fields of 10^5 V/cm, and the expected large $\chi^{(3)}$ values associated with these dyes, this term can become significant for a cellular membrane. It should be noted that the above equation is nonlinear and that the actual response is dependent upon the relative contributions of $\chi^{(2)}$ and $\chi^{(3)}$ for a given dye, as well as the magnitude of the field. This function may be quasilinear in some regions of potential, but some care must be given in this application. These dependencies are the subject of ongoing work in our laboratory.

It should be noted that this scenario differs markedly from that in an electric field induced second harmonic (EFISH) experiment. In the latter, an applied electric field organizes a random distribution of molecules and is solely responsible for any observed second harmonic signal. For our case, the membrane staining dyes have a structural alignment within the membrane in the absence of a field, as indicated by a nonzero steady-state, field independent second harmonic signal. In work to be published we show through polarization anisotropy measurements that this is indeed the case.

4.2 SHG Enhancements from Gold Nanoparticles

In an effort to increase the contrast in SHIM we looked for enhancements in the signal levels from the interaction of the ANEP chromophore with metallic nanoparticles at membranes. In some of our earlier work we showed that such enhancements were indeed possible.^{43,44} The results from a first, simple experiment are shown in Figure 7. Here both the SHG and TPEF images were taken of N1E-115 neuroblastoma cells in normal buffer stained with the JPW-2080 dye, then approximately 1 μmol of 30 nm gold colloids were added and allowed to equilibrate for about 30 min. The SHG and TPEF were measured and are shown in the bottom panels. Interaction of the dye with the nanoparticles will be manifested in both an SHG enhancement as well as a fluorescence quenching, as the metal provides an additional nonradiative pathway. In this case integration of the whole cell showed that the fluorescence was quenched by approximately 20%, while the SHG was enhanced threefold.

While this method demonstrates the promise in using this method, the process is slow and the interaction at the nanoparticle interaction at the membrane is somewhat ill-defined. For example, we do not know the average distance of the colloids to the imbedded dye molecules or how this distribution varies. To improve this situation,⁴⁵ we synthesized a new type of conjugate particle: 100 nm gold colloids were coated with a polymerized mixture of styrene and methacrylic acid⁴⁶ and then linked to the same styryl chromophore via a succinimidylyl ester. The polymer coating was examined by transmission electron microscopy and consisted of a regular 4 nm

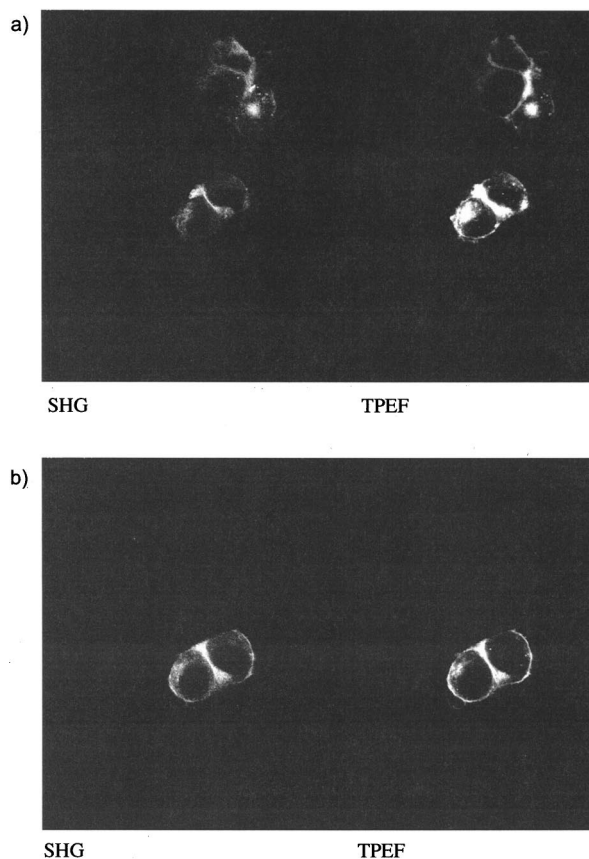


Fig. 7 SHG and TPEF imaging of undifferentiated N1E-115 cells to determine the SHG enhancement due to the addition of 30 nm gold colloids. Top panel (a) is prior to the addition of colloids. The bottom panel was obtained 30 min following the addition of the colloids. The top cells detached when the colloids were added. A 40 \times , 0.8 NA water immersion lens was used for the excitation.

thick layer. A convenient method to quantitatively assay SHG intensity dependence between different samples labeled with the same chromophore is to normalize to the TPEF intensity, as discussed above. This method works because both contrast mechanisms arise from the styryl dye and is appropriate when the TPE spectrum is unchanging. We use this approach here to measure the SHG enhancement of the dye/nanoparticle conjugate relative to the unconjugated dye. The L1210 cells were first stained with Di-2-ANEPPA which has the same chromophore shown earlier but has a terminal amine for the conjugation chemistry. A composite SHG (left panel) and TPEF (right panel) image of live L1210 lymphocytes is shown in Figure 8(a). The process was then repeated for L1210 cells stained with the dye/nanoparticle conjugate and a composite of 3 SHG and TPEF frames is shown in Figure 8(b). In each case, following background subtraction, the SHG/TPEF ratio was measured on a cell by cell basis and 30 were used for the average. The enhancement due to the gold particle is then expressed by

$$\text{SHG}_{\text{enhancement}} = \frac{[\text{SHG/TPEF}]_{\text{gold}}}{[\text{SHG/TPEF}]_{\text{no gold}}} = 21 \pm 9. \quad (9)$$

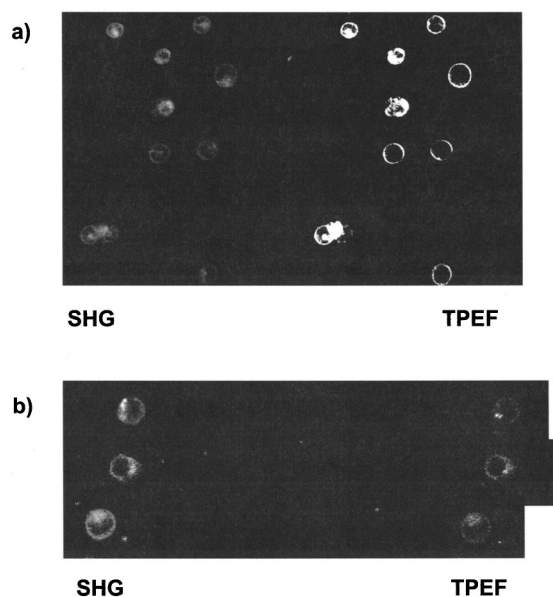


Fig. 8 SHG and TPEF imaging of L1210 lymphocytes: (a) stained with ANEPPS and (b) composite image of cells labeled with dye-nanoparticle conjugates.

A drawback of the ratiometric method described above is that the extent of SHG enhancement and fluorescence quenching due to the gold particle cannot be directly separated. It is well known that fluorescence quenching due to metals is highly distance dependent⁴⁷ and that there can also exist a fluorescence enhancement due to surface plasmon resonance.⁴⁸ To account for these uncertainties, the fluorescence lifetime was measured for both the normal Di-2-ANEPPA and the dye/nanoparticle conjugate. For convenience, these measurements were performed as an ensemble average of PC liposomes stained with these dyes. The measurements were made using time correlated single photon counting and the instrument response function was determined to be 400 ps. Following deconvolution of the IRF and then exponential fitting, the respective lifetimes for Di-2-ANEPPA and the dye-nanoparticle conjugate were 2.65 and 2.35 ns, as shown in the emission decays in Figure 9. This can be interpreted by inspection of the Jablonski diagram in Figure 10. In the top panel, the situation is shown for the dye alone, where the relative fluorescence quantum efficiency can be expressed as

$$\phi_{fl} = \frac{k_f}{k_f + k_{isc}}, \quad (10)$$

where k_f and k_{isc} are the decay rates for fluorescence and intersystem crossing to the triplet state. For the case of the conjugate particles the quantum yield is given by

$$\phi_f = \frac{k_f}{k_f + k_{isc} + k_m}, \quad (11)$$

where k_m is the decay rate to the metal electron sea. Given that the chromophore is nominally unchanged for these two cases, the extent of quenching is given by the ratio of fluorescence lifetimes or

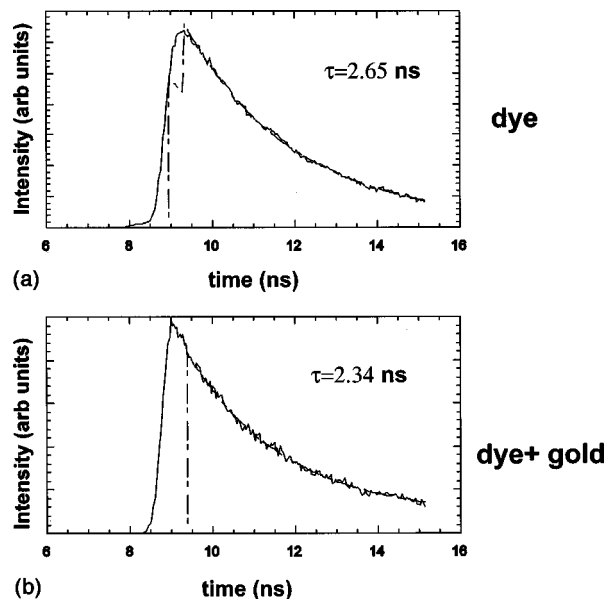


Fig. 9 Fluorescence lifetime measurements of PC liposomes labeled with (a) unconjugated dye and (b) dye-nanoparticle conjugates.

$$\frac{\phi_{norm}}{\phi_{gold}} = \frac{\tau_{norm}}{\tau_{gold}} = 1.2 \quad (12)$$

or approximately 20%, relative to an approximately 20-fold SHG enhancement. Therefore the increase in the SHG/TPEF ratio can be ascribed largely to SHG enhancement rather than

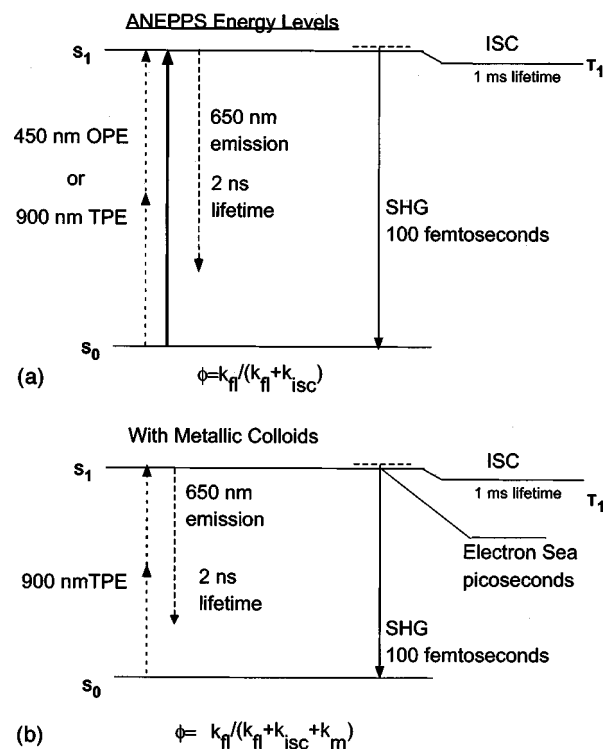


Fig. 10 Jablonski diagram showing the energy levels and decay pathways for (a) unconjugated dye and (b) dye-nanoparticle conjugates, and the expressions for the fluorescence quantum yield, ϕ .

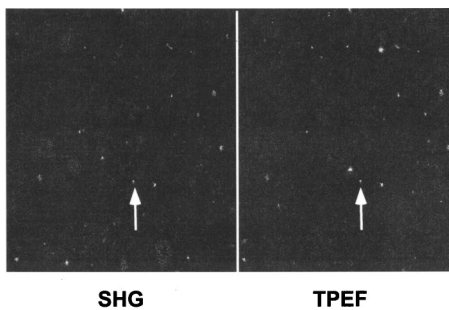


Fig. 11 SHG and TPEF images of dye-nanoparticle conjugates in water. The arrows point to the same particles in both images for reference.

fluorescence quenching from the gold. To verify that the observed SHG signals depended on both the dye and gold nanoparticles the following controls were done. In the left and right panels of Figure 11 are shown the respective SHG and TPEF images of the dye/nanoparticle conjugates in an aqueous environment. We believe that each small bright point corresponds to a single particle (~ 100 nm diameter) or a small aggregate. As a control, the laser was taken out of mode-locking operation and the respective SHG and TPEF signals disappeared, indicating the contrast arose from a nonlinear process rather than signal bleedthrough from a linear scattering process. In addition, the particles bleached after prolonged exposure, indicating the signal depended upon the dye and gold particle being present (free dye produces no SHG). Excitation of unlabeled gold particles in aqueous solution under identical imaging conditions produced no observable second harmonic signal. (It should be noted that SHG can be observed from bare colloidal gold particles with higher photon flux than were used in this experiment.) Similarly, 100 nm latex beads which were conjugated to Di-2-ANEPPA (via the same chemistry as the 100 nm gold particles) in water produced no observable SH signals in either an ensemble average or imaging experiment. Based on our limits of detection, we can place a lower bound on the gold enhancement of the dye SHG of a factor of 100 relative to the latex-bound dye. These controls indicate that the second harmonic signals arose from the dye conjugated to the gold nanoparticle and that the signals arise from enhancement from the gold. Given the excitation wavelength (~ 840 nm), we suggest this is due at least in part to a surface plasmon enhancement arising from a two-photon process. The presence of the TPEF signal is interesting since the free dye in water has no fluorescence quantum yield, presumably due to nonradiative losses arising from extensive hydrogen bonding. Although we do not know the number of dye molecules per nanoparticle, this result suggests that dye molecules are sufficiently close together to screen each other from the water solvent, and can thus fluoresce. Alternatively, the dye may become intercalated in the polymer coating.

4.3 SHG Imaging of Endogenous Collagen

In this work presented so far, the cells were stained with a lipophilic, voltage sensitive styryl dye to generate sufficient contrast. These dyes display a resonance enhancement of SHG due to the proximity of an excited state close to the second harmonic wavelength. Thus there is always some col-

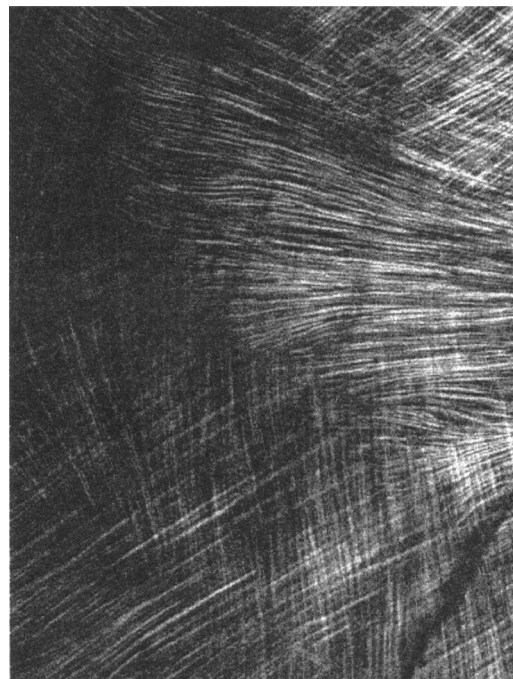


Fig. 12 SHG image of a zebrafish scale. The signal arises from the endogenous collagen in the matrix and no exogenous labels were used. The power level was approximately 1 mW.

lateral TPEF, which, as has been shown, can often be used to advantage in interpreting the SHG. Although out-of-plane photobleaching and phototoxic effects are reduced in nonlinear optical excitation schemes, in-plane damage still results, largely from the formation of singlet oxygen free radicals upon photobleaching of fluorescent dyes. But, inherently, it should be possible to obtain SHG without having to resort to resonance enhancement of exogenous dyes. Such signals would not involve population of an excited state and therefore would show no photobleaching or phototoxicity. Thus it would be highly desirable to obtain high-resolution (near diffraction limited) images with high contrast on purely endogenous biological samples, since phototoxic effects would be virtually eliminated. We have indeed achieved this goal in visualizing several structural proteins.

It has been known for some time from polarization microscopy that structural proteins organize to form highly birefringent structures.⁴⁹ There has been some previous work using SHG to image endogenous tissue. In a series of rigorous experiments, Freund et al. used SHG microscopy in 1986 to study the endogenous collagen structure in a rat tail tendon at approximately $50 \mu\text{m}$ resolution.¹⁷ More recently, in a reflection mode setup, Alfano and coworkers used stage scanning SHG to image chicken muscle and connective tissue, where frame rates of several hours were required.⁵⁰ We have extended this idea to imaging endogenous proteins on our laser scanning transmission mode microscope and have achieved higher resolution (ca. $1 \mu\text{m}$) and much higher rates of image acquisition (1 frame per second). This rate is only limited by our scanner speed as the signals are sufficiently intense to allow greater acquisition rates. We have obtained bright, three-dimensional images of several tissues. An example of which is shown in Figure 12 of a zebrafish scale. Scales con-

sist largely of keratin and collagen, the latter is known to possess a large second-order response, and is likely the contrast generating molecule in this image. Several controls indicated this image was produced exclusively at the expected second harmonic wavelength with no autofluorescence background. It should be noted that in this form SHIM is an intrinsically bleachless technique. This method has been extended to several other structural proteins and will be the subject of a forthcoming publication.

5 Perspectives

Since SHG is a nonlinear form of optical excitation, it is natural to place this imaging scheme in the context of two and three photon-excited fluorescence. Due to the peak power requirement, SHIM retains all the benefits of multiphoton excited fluorescence imaging, and likewise, since the excitation is typically in the near infrared, excellent penetration into thick and turbid samples is obtainable. Indeed, in work to be published, we show optical sectioning through 600 μm of muscle tissue. At the same excitation wavelength, the resolution of SHG and TPEF is also going to be comparable since the power dependence is identical.

The differences in the method of contrast generation can lead to differently appearing images of the same cell. We showed that if a membrane bound dye equally stains both leaflets of a membrane, that within the electric dipole approximation, the SHG image should disappear while the fluorescence is not phase sensitive and will persist. Alternatively, at high dye concentrations, aggregation can occur and will lead to fluorescence quenching. However, the SHG scales as the square of the surface concentration and will actually lead to brighter signals. This prediction will be demonstrated in a forthcoming publication. Finally, SHG will only occur at a membrane, while in theory, other membrane bound dyes may have nonzero fluorescence quantum yield in the aqueous cytosol.

A potential drawback of SHIM is that somewhat higher power is needed relative to TPEF to obtain similar brightness, on the order of fivefold. More rigorous predictions have been worked out by Mertz and coworkers.⁵¹ However, when working further in the infrared, ($\lambda > 850 \text{ nm}$) it is well documented that the photodamage considerations are greatly reduced.^{52,53} The development of better dyes will improve this situation further. Another area of improvement could lie in taking advantage of the temporal coherence of the SHG signal, thus removing the longer lived fluorescence (nanoseconds) as well as background light. Further improvements could be achieved by the use of UV sensitive avalanche photodiodes.

Perhaps the most unique aspect of the SHIM approach lies in the ability to probe membrane potential at greater sensitivity than possible by fluorescence methods. Although the absolute signal levels may currently be smaller than fluorescence, the enhanced sensitivity of SHG to voltage predicts significantly higher signal-to-noise ratios for optical recording of electrical activity. This feature leads us to believe SHIM will become a powerful tool for probing physiology in live cells and tissues.

Acknowledgments

We gratefully acknowledge financial support under ONR N0014-98-1-0703, NIGMS 5 R01-GM35063, the NSF Academic Research Infrastructure DBI-9601609, and the State of Connecticut Critical Technology program.

References

1. W. Denk, J. H. Strickler, and W. W. Webb, "Two-photon laser scanning fluorescence microscopy," *Science* **248**, 73–76 (1990).
2. W. Denk, M. Sugimori, and R. Linas, "Two types of calcium response limited to single spines in cerebellar Purkinje cells," *Proc. Natl. Acad. Sci. U.S.A.* **92**, 8279–8282 (1995).
3. M. Maletic-Savatic, R. Malinow, and K. Svoboda, "Rapid dendritic morphogenesis in CA1 hippocampal dendrites induced by synaptic activity," *Science* **283**, 1923–1927 (1999).
4. S. M. Potter, C.-M. Wang, P. A. Garrity, and S. E. Fraser, "Intravital imaging of green fluorescent protein using two-photon laser-scanning microscopy," *Gene* **173**, 25–31 (1996).
5. S. Maiti, J. B. Shear, R. M. Williams, W. R. Zipfel, and W. W. Webb, "Measuring serotonin distribution in live cells with three-photon excitation," *Science* **275**, 530–532 (1997).
6. K. D. Niswender, S. M. Blackman, L. Rohde, M. A. Magnuson, and D. W. Piston, "Quantitative imaging of green fluorescent protein in cultured cell: comparison of microscopic techniques, use in fusion proteins, and detection limits," *J. Microsc.* **180**(2), 109–116 (1995).
7. G. H. Patterson, S. M. Knobel, W. D. Sharif, S. R. Kain, and D. W. Piston, "Use of the green fluorescent protein and its mutants in quantitative fluorescence microscopy," *Biophys. J.* **73**, 2782–2790 (1997).
8. D. Kleinfeld, P. P. Mitra, F. Helmchen, and W. Denk, "Fluctuations and stimulus-induced changes in blood flow observed in individual capillaries in layers 2 through 4 of rat neocortex," *Proc. Natl. Acad. Sci. U.S.A.* **95**, 15741–15746 (1998).
9. D. L. Wokosin, V. E. Centonze, S. Crittenden, and J. White, "Three-photon excitation fluorescence imaging of biological specimens using an all-solid state laser," *Bioimaging* **4**, 208–214 (1996).
10. D. A. Kleinman, "Nonlinear dielectric polarization in optical media," *Phys. Rev.* **126**, 1977–1979 (1962).
11. N. Bloembergen, R. K. Chang, S. S. Jha, and C. H. Lee, "Optical second-harmonic generation in reflection from media with inversion symmetry" *Phys. Rev.* **174**, 19813–19822 (1968).
12. Y. R. Shen, "Surface properties probed by second-harmonic and sum-frequency generation," *Nature (London)* **337**, 519–525 (1989).
13. K. B. Eisenthal, "Liquid interfaces probed by second-harmonic and sum-frequency spectroscopy," *Chem. Rev.* **96**, 1343–1360 (1996).
14. R. Hellwarth and P. Christensen, "Nonlinear optical microscopic examination of structure in polycrystalline ZnSe," *Opt. Commun.* **12**, 318–322 (1974).
15. C. J. R. Sheppard, R. Kompfner, J. Gannaway, and D. Walsh, "Scanning harmonic optical microscope," *IEEE J. Quantum Electron.* **13E**, 100D (1977).
16. R. Gauderon, P. B. Lukins, and C. J. R. Sheppard, "Three-dimensional second harmonic generation imaging with femtosecond laser pulses," *Opt. Lett.* **23**, 1209–1211 (1998).
17. I. Freund, M. Deutsch, and A. Sprecher, "Connective tissue polarity," *Biophys. J.* **50**, 693–712 (1986).
18. Th. Raising, J. Huang, A. Lewis, T. Stehlin, and Y. R. Shen, "In situ determination of induced dipole moments of pure and membrane-bound retinal chromophores," *Phys. Rev. A* **40**, 1684–1687 (1989).
19. O. Bouevitch, A. Lewis, I. Pinevsky, J. P. Wuskell, and L. M. Loew, "Probing membrane potential with non-linear optics," *Biophys. J.* **65**, 672–679 (1993).
20. I. Ben-Oren, G. Peleg, A. Lewis, B. Minke, and L. Loew, "Infrared nonlinear optical measurements of membrane potential in photoreceptor cells," *Biophys. J.* **71**, 1616–1620 (1996).
21. P. J. Campagnola, M. D. Wei, A. Lewis, and L. M. Loew, "High resolution non-linear optical microscopy of living cells by second harmonic generation," *Biophys. J.* **77**, 3341–3349 (1999).
22. Y. Huang, A. Lewis, and L. M. Loew, "Non-linear optical properties of potential sensitive styryl dyes," *Biophys. J.* **53**, 665–670 (1988).
23. S. R. Marder, D. N. Beratan, and L.-T. Cheng, "Approaches for optimizing the first electronic hyperpolarizability of conjugated organic molecules," *Science* **252**, 103–106 (1991).
24. S. R. Marder, J. W. Perry, and W. P. Schaeffer, "Synthesis of organic

- salts with large second-order optical nonlinearities," *Science* **245**, 626–628 (1989).
25. C. R. Moylan, R. J. Twieg, V. Y. Lee, S. A. Swanson, K. M. Betterton, and R. D. Miller, "Nonlinear optical chromophores with large hyperpolarizabilities and enhanced thermal stabilities," *J. Am. Chem. Soc.* **115**, 12599–12600 (1993).
 26. C. M. Whitaker, E. V. Patterson, K. L. Kott, and R. J. McMahon, "Nitrogen and oxygen donor in nonlinear optical materials: effects of alkyl vs phenyl substitution on the molecular hyperpolarizability," *J. Am. Chem. Soc.* **118**, 9966–9973 (1996).
 27. P. J. A. Kenis, O. F. J. Noordman, S. Houbrechts, G. J. van Hummel, S. Harkema, F. C. J. M. Veggel, K. Clays, J. F. J. Engbersen, A. Persoons, N. F. van Hulst, and D. N. Reinhoudt, "Second-order nonlinear optical properties of the four tetranitrotetrapropoxycalix[4]arene conformers," *J. Am. Chem. Soc.* **120**, 7875–7883 (1998).
 28. I. D. L. Albert, T. J. Marks, and M. A. Ratner, "Remarkable NLO response and infrared absorption in simple twisted molecular π -chromophores," *J. Am. Chem. Soc.* **120**, 11174–11181 (1998).
 29. R. R. Tykwinski, U. Gubler, R. E. Martin, F. Diederich, C. Bosshard, and P. Gunter, "Structure-property relationships in third-order nonlinear optical chromophores," *J. Phys. Chem. B* **102**, 4451–4465 (1998).
 30. T. Verbiest, S. V. Elshocht, M. Kauranen, L. Hellemans, J. Snauwaert, C. Nuckolls, T. J. Katz, and A. Persoons, "Strong enhancement of nonlinear optical properties through supramolecular chirality," *Science* **282**, 913–915 (1998).
 31. J. L. Oudar and D. S. Chemla, "Hyperpolarizabilities of the nitroanilines and their relations to the excited state dipole moment," *J. Chem. Phys.* **66**, 2664–2468 (1977).
 32. L. M. Loew and L. Simpson, "Charge shift probes of membrane potential. A probable electrochromic mechanism for ASP probes on a hemispherical lipid bilayer," *Biophys. J.* **34**, 353–365 (1981).
 33. T. F. Heinz, C. K. Chen, D. Ricard, and Y. R. Shen, "Spectroscopy of molecular monolayers by resonant second-harmonic generation," *Phys. Rev. Lett.* **48**, 478–481 (1982).
 34. G. T. Boyd, Th. Rasing, R. R. Leite, and Y. R. Shen, "Local-field enhancement on rough surfaces of metals, semimetals, and semiconductors with the use of optical second harmonic generation," *Phys. Rev. B* **30**, 519–526 (1984).
 35. M. Moskovits, "Surface enhanced spectroscopy," *Rev. Mod. Phys.* **57**, 783–826 (1985).
 36. S. R. Emory, W. E. Haskins, and S. Nie, "Direct observation of size-dependent optical enhancement in single metal nanoparticles," *J. Am. Chem. Soc.* **120**, 8009–8010 (1998).
 37. L. M. Loew, "Voltage-sensitive dyes and imaging neuronal activity," *Neuroprotocols* **5**, 72–79 (1994).
 38. L. Moreaux, O. Sandre, M. Blanchard-desce, and J. Mertz, "Membrane imaging by simultaneous second-harmonic generation and two-photon microscopy," *Opt. Lett.* **25**, 320–322 (2000).
 39. L. M. Loew, "Confocal microscopy of potentiometric fluorescent dyes," in *Cell Biological Applications of Confocal Microscopy, Methods in Cell Biology*, B. Matsumoto, Ed., Vol. 38, pp. 194–209, Academic, Orlando (1993).
 40. L. M. Loew, "Measuring membrane potential in single cells with confocal microscopy," in *Cell Biology: A Laboratory Handbook*, J. E. Cellis, Ed., Vol. 3, pp. 375–379, Academic, Orlando (1998).
 41. J. C. Conboy and G. L. Richmond, "Examination of the electrochemical interface between two immiscible electrolyte solutions by second harmonic generation," *J. Phys. Chem.* **101**, 983–990 (1997).
 42. Y. R. Shen, *The Principles of Non-linear Optics*, Wiley, New York (1984).
 43. G. Peleg, A. Lewis, O. Bouvitch, L. Loew, D. Parnas, and M. Linai, "Gigantic optical non-linearities from nanoparticle-enhanced molecular probes with potential for selectively imaging the structure and physiology of nanometric regions in cellular systems," *Bioimaging* **4**, 215–224 (1996).
 44. G. Peleg, A. Lewis, M. Linial, and L. M. Loew, "Non-linear optical measurement of membrane potential around single molecules at selected cellular sites," *Proc. Natl. Acad. Sci. U.S.A.* **96**, 6700–6704 (1999).
 45. H. A. Clark, P. J. Campagnola, J. P. Wuskell, A. Lewis, and L. M. Loew, "Second harmonic generation properties of fluorescent polymer encapsulated gold nanoparticles," *J. Am. Chem. Soc.* **122**, 10234–10235 (2000).
 46. L. Quaroni and G. Chumanov, "Preparation of polymer-coated functionalized silver nanoparticles," *J. Am. Chem. Soc.* **121**, 10642–10643 (1999).
 47. B. Zelent, J. Kusba, I. Gryczynski, M. L. Johnson, and J. R. Lakowicz, "Distance-dependent fluorescence quenching of *p*-Bis[2-(5-phenyloxazolyl)]benzene by various quenchers," *J. Phys. Chem.* **100**, 18592–18602 (1996).
 48. K. Sokolov, G. Chumanov, and T. M. Cotton, "Enhancement of molecular fluorescence near the surface of metal films," *Anal. Chem.* **70**, 3898–3905 (1998).
 49. S. Inoue, *Video Microscopy*, Plenum, New York (1986).
 50. Y. Guo, P. P. Ho, H. Savage, D. Harris, P. Sacks, S. Schantz, F. Liu, N. Zhadin, and R. R. Alfano, "Second-harmonic tomography of tissues," *Opt. Lett.* **22**, 1323–1325 (1997).
 51. L. Moreaux, O. Sandre, S. Charpak, M. Blanchard-Desce, and J. Mertz, "Coherent scattering in multi-harmonic light microscopy," *Biophys. J.* **80**, 1568–1574 (2001).
 52. K. König, P. T. C. So, W. W. Mantulin, and E. Gratton, "Cellular response to near-infrared femtosecond laser pulses in two-photon microscopes," *Opt. Lett.* **22**, 135–136 (1997).
 53. K. König, T. W. Becker, P. Fischer, I. Riemann, and K.-J. Halhuber, "Pulse-length dependence of cellular response to intense near-infrared laser pulses in multiphoton microscopes," *Opt. Lett.* **24**, 113–115 (1999).